Surface & Coatings Technology 393 (2020) 125721

Contents lists available at ScienceDirect

Surface & Coatings Technology

journal homepage: www.elsevier.com/locate/surfcoat

Hall-effect studies of modification of HgCdTe surface properties with ion implantation and thermal annealing

A.G. Korotaev[a], I.I. Izhnin[a,b], K.D. Mynbaev[c,*], A.V. Voitsekhovskii[a], S.N. Nesmelov[a], S.M. Dzyadukh[a], O.I. Fitsych[b], V.S. Varavin[d], S.A. Dvoretsky[a,d], N.N. Mikhailov[d], M.V. Yakushev[d], O.Yu. Bonchyk[e], H.V. Savytskyy[e], Z. Swiatek[f], J. Morgiel[f]

[a] National Research Tomsk State University, 36 Lenin Av., 634050 Tomsk, Russia
[b] Scientific Research Company "Electron-Carat", 202 Stryjska Str., 79031 Lviv, Ukraine
[c] ITMO University, 49 Kronverkskiy pr., 197101 Saint–Petersburg, Russia
[d] A.V. Rzhanov Institute of Semiconductor Physics of SB RAS, 13 Lavrent'ev Av., 630090 Novosibirsk, Russia
[e] Ya.S. Pidstryhach Institute for Applied Problems of Mechanics and Mathematics NASU, 3b Naukowa Str, 79060 Lviv, Ukraine
[f] Institute of Metallurgy and Material Science PAN, 25 Reymonta Str., 30-059 Krakow, Poland

ARTICLE INFO

Keywords:
Ion implantation
Surface modification
HgCdTe
Defects

ABSTRACT

Results of the Hall-effect studies of surface properties of *n*–type HgCdTe films modified with arsenic ion implantation and thermal annealing are reported on. A complete annihilation of implantation-induced extended defects (dislocation loops), quasi-point defects and related donor centers was observed as a result of a two-stage arsenic activation annealing. A high degree of activation of implanted arsenic was achieved with the annealing. In some cases, the annealing was found to lead to the modification of the properties of the 'base' layers not affected by implantation due to activation of uncontrolled acceptor defects and resulting changes in the degree of electrical compensation.

1. Introduction

HgCdTe solid solutions have been used in photodetectors operating in the long-wavelength infrared (LWIR) range for over 50 years [1]. The two most common technologies of HgCdTe-based photodiodes are *n*-on-*p* and *p*-on-*n* planar architectures. For these architectures, in the 'base' layer (*p*- and *n*-type, respectively), a highly doped area (n^+- and p^+-type, respectively) is fabricated with ion implantation. The *n*-on-*p* planar technology is the oldest one; these photodiodes are formed in *p*-type 'base' where mercury vacancies (V_{Hg}) serve as acceptors, and the n^+-type doping is achieved with ion implantation of boron [2]. The use of V_{Hg} as the *p*-type intrinsic dopant, however, is known to degrade the electron lifetime due to the introduction of the centers of Shockley-Read recombination, so the resulting detectors exhibit high dark current. For this reason, *p*-on-*n* architectures have been gaining more and more interest in the last 20 years. Compared with the *n*-on-*p* technology, the *n*-type 'base' (active layer) is doped extrinsically, and the minority-carrier lifetime is governed by band-to-band CHCC recombination, providing the highest lifetimes possible. Additionally, the *p*-on-*n* technology decreases the serial resistance by means of employing high-mobility majority carriers (electrons) [3]. As a result, the *p*-on-*n* architecture allows for a decreased dark current, and thus, for improved operability at high temperature or for higher detector cut-off wavelength.

Typically, p^+-on-*n* junctions are fabricated in HgCdTe with the use of arsenic ion implantation followed by thermal activation of implanted species [4–6]. Fabrication of such p^+-on-*n* diodes appears to be more challenging than traditional boron-implantation n^+-*p* technology. Ion implantation produces in the surface layer of HgCdTe both extended and quasi-point radiation defects (see, e.g., Refs. [7, 8]). Interstitial mercury atoms Hg_I released as a result of implantation damage interact with these defects and form two types of electrically-active donor centers [9,10], so irrespective of the dopant used, the as-implanted layer always exhibits n^+-type conductivity. Thus, fabrication of p^+-*n* structure requires an annealing, which should activate implanted arsenic and annihilate radiation defects while eventually maintaining original electrical properties of the *n*-'base'. For an effective annealing, it is necessary to know the exact nature of the donor defects, their (and that of the dopant) location in the implanted material, and how the annealing affects their pattern. The most part of the earlier works was focused on structural studies of the implantation-damaged area and on its transformation under arsenic activation annealing [3–8]. Detailed

* Corresponding author.
E-mail address: mynkad@mail.ioffe.ru (K.D. Mynbaev).

https://doi.org/10.1016/j.surfcoat.2020.125721
Received 14 October 2019; Received in revised form 26 March 2020; Accepted 31 March 2020
Available online 01 April 2020

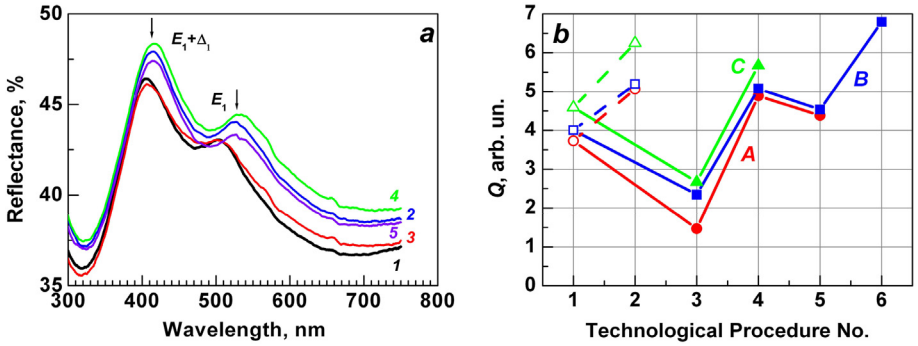

Fig. 1. Optical reflectance spectra of sample *A* recorded at 300 K (*a*): after the growth (*1*); after 'activation' annealing performed on non-implanted sample (*2*); after ion implantation (*3*); after activation annealing of the implanted sample (*4*); after additional '*p*-type' annealing of the implanted and activation-annealed sample (*5*). Image (*b*) shows changes in the value of 'peak sharpness' *Q* after the treatments for all three samples. For sample *B*, the value of *Q* is also shown after the removal of the graded-gap surface layer after all annealings ('Procedure No. 6').

electrical studies, in their turn, were performed only on arsenic-implanted n^+–p junctions formed in a *p*–type 'base' [9,10]. The purpose of this work was to study the effect of various types of thermal treatment on the properties of arsenic-implanted HgCdTe films and on the behavior of the implantation-induced donor defects in the *n*–type 'base'.

2. Experimental details

The films were grown by molecular-beam epitaxy (MBE) at A.V. Rzhanov Institute of Semiconductor Physics (Novosibirsk, Russia) on (013) CdTe/ZnTe/Si substrates with the growth cycle controlled in situ by means of an ellipsometer [11]. The total thickness of the films was 7–9 μm. Their 'absorber' layers with CdTe molar fraction (composition) $x \approx 0.22$ were in situ covered with graded-gap protective layers with composition ~0.46 at the surface. The thickness of the graded-gap layers was ~0.4 μm. The films were doped with indium (donor in HgCdTe) during the growth. The indium concentration C_{In} set during the growth equaled $(1–1.5)\cdot10^{15}$ cm^{-3} in samples *A* and *B* and $5\cdot10^{15}$ cm^{-3} in sample *C*. The doping resulted in the electron concentration in the active layer equaling $8.13\cdot10^{14}$ cm^{-3} in sample *A*, $8.17\cdot10^{14}$ cm^{-3} in sample *B* and $3.9\cdot10^{15}$ cm^{-3} in sample *C*.

Ion implantation was performed with As^+ ions with energy 190 keV and fluence 10^{14} cm^{-2} using IMC200 (Ion Beam Services, France) installation. The projected and total ion range for arsenic implanted in this regime equaled ~93 nm and ~350 nm, respectively [9]. Arsenic concentration in the films was determined with Secondary Ion Mass–Spectroscopy (SIMS) using a Cameca IMS–6F machine with arsenic detection limit ~10^{16} cm^{-3}. Transmission Electron Microscopy (TEM) studies of the microstructure of the implanted material were performed in bright-field mode with the use of Tecnai G2 F20, FEI Company microscope. Thin foils for TEM observations were cut out using FEI Quanta 200 dual-beam focused-ion (Ga^+) beam machine equipped with OmniprobeTM lift-out system. Electrical properties of the samples were investigated by measuring the magnetic field dependences of the Hall coefficient $R_H(B)$ and the conductivity $\sigma(B)$ in fields $B = 0.01–1.5$ T at $T = 77$ K. The data of these measurements were analyzed with the use of the discrete mobility spectrum analysis (DMSA) [9,10], which allows for determining the number of carrier species and their parameters: concentration, mobility and partial conductivity. Optical reflectance spectra were recorded in 300–800 nm wavelength range with the step 0.2 nm at $T = 300$ K using Shimadzu UV-3600 (Japan) spectrometer. The spectra were recorded with the use of the reflectance measurement console with 5 mm diaphragm. The incident light was hitting the surface of the sample at the angle 5° in respect to the normal to the surface.

Two types of annealing were applied to the implanted samples: 1) conventional two-stage activation annealing (~360 °C, 2 h/~220 °C, 24 h) under saturated mercury pressure [3,4,7] (to test the effect of this annealing on the properties of the material, a piece of each as-grown film was also annealed in this regime without implantation); 2) annealing for attaining vacancy-doped *p*-type HgCdTe [12]; this annealing was performed under low mercury pressure in helium atmosphere (230 °C, 22 h).

3. Experimental results and discussion

3.1. Optical reflectance

The structural perfection of the surface of the films and its modification by the implantation and annealings were studied with optical reflectance. In HgCdTe reflectance spectra in the visible range, two distinct peaks are typically observed, E_1 and $E_1 + \Delta_1$, which originate in transitions $\Lambda_{4,5} \rightarrow \Lambda_6$ and $\Lambda_6 \rightarrow \Lambda_6$ [13,14]. The energy position and the shape of the peaks give information on the value of the energy gap (and, correspondingly, chemical composition) and the structural perfection of the material, respectively. To assess changes in the shape of the peaks after ion implantation and annealing(s), a 'peak sharpness' $Q = \Delta R / R_1$ parameter was used, where ΔR was the value of the 'dip' between the peaks and R_1 was the reflectance in the maximum of the peak E_1 [15]. An example of reflectance spectra transformations is given in Fig. 1(a) for sample *A*. Changes in values of *Q* for all three samples are summarized in Fig. 1(b). Here, the dashed lines trace the changes in *Q* after the 'activation' annealing of the as-grown (non-implanted) samples, while the solid lines show the changes after implantation-related technological procedures performed on the sample. All these lines are given solely as a guide for the eye.

The changes in the value of *Q* for all three studied samples appeared to be similar. 'Activation' annealing of non-implanted samples increased *Q* and also lead to decrease in composition of the graded-gap surface layer due to the diffusion of Cd and Hg. After ion implantation, *Q* became significantly smaller than that in the as-grown sample, which was indicative of the substantial disruption of the crystal lattice. After activation annealing, the values of *Q* for all three samples substantially increased and approached those typical of films annealed without implantation; this was clearly indicative of the annihilation of implantation-induced structural defects. Additional '*p*-type' annealing of implanted and activation-annealed samples, which was performed for samples *A* and *B*, lead to some decrease in *Q* values. This could be related to some loss of mercury from the surface of the material under this type of annealing. The removal of the graded-gap surface layer with chemical etching drastically increased the value of *Q*, which was indicative of much better structural perfection of the active layer of the film in respect to its surface layer.

3.2. The Hall-effect and TEM studies

Electrical properties of the films were studied with variable-field Hall-effect measurements. For the as-grown film and for the films subjected to technological procedures 2 to 4, R_H was negative for all the studied magnetic fields with an inflection observed at B~0.1 T, so these were 'pure' *n*-type samples with conductivity dominated by electrons with high and low mobility. Sample *C* demonstrated rather weak $R_H(B)$ dependence for the as-grown film and films after implantation and post-

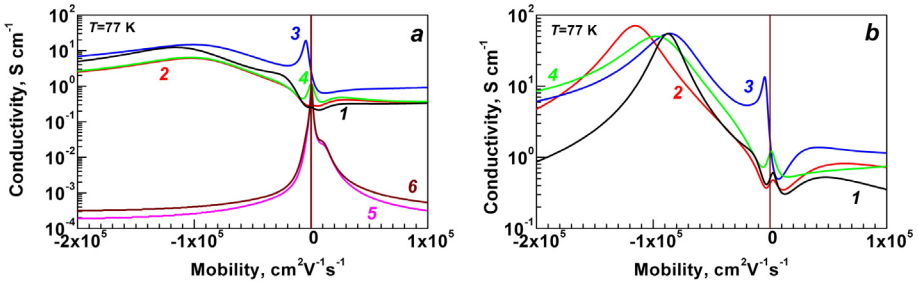

Fig. 2. Mobility spectrum envelopes for sample *A* (*a*) and sample *C* (*b*): after the growth (*1*); after 'activation' annealing performed on non-implanted sample (*2*); after ion implantation (*3*); after activation annealing of the implanted sample (*4*); after '*p*-type' annealing of the implanted and activation-annealed sample (*5*); after the removal of the graded-gap surface layer from the annealed sample (*6*).

implantation annealing. This could possibly be related to different contribution to conductivity by electrons with high and low mobility, which originate in corresponding defects formed as a result of the treatment.

Examples of transformation of primary mobility spectrum envelopes (MSE) after various technological procedures are given in Fig. 2 for samples *A* and *C*. The shapes of the MSE of the as-grown films (curves *1*) were indicative of the presence of at least two types of electrons (a peak and a shoulder at the negative part of the mobility axis, ~80,000–100,000 cm^2 / (V·s) and ~10,000–20,000 cm^2 / (V·s), respectively) (the 'negative' part of the mobility axis was introduced exclusively for the clarity of presentation, so that electron and hole mobility peaks would not superimpose). For sample *A*, DMSA of the parameters of the carriers showed that conductivity was dominated by electrons with the average (calculated for the whole thickness of the sample) concentration n_{av} = 8.1·10^{14} cm^{-3} and mobility μ_n = 107,100 cm^2 / (V·s). The electron concentration appeared to be slightly smaller than C_{In} ((1–1.5)·10^{15} cm^{-3} for samples *A* and *B*), which could be explained by partial electrical compensation of donors by residual acceptors. In sample *C* (C_{In} ≈ 5·10^{15} cm^{-3}) the conductivity was dominated by electrons with n_{av} = 3.9·10^{15} cm^{-3} and μ_n = 87,500 cm^2 / (V·s). Also, electrons with lower mobility were revealed; their average concentration in sample *A* equaled n_h = 4.2·10^{14} cm^{-3}; mobility, μ_{nh} = 3,930 cm^2 / (V·s). The mobility of lower-mobility electrons in as-grown samples *A* and *B* was somewhat lower than that in as-grown sample *C* (μ_{nh} = 12,200 cm^2 / (V·s)). These electrons belonged to the transitional substrate/epitaxial film layer typical of MBE-grown HgCdTe [16,17]. The total conductivity due to holes was less than 3%, so the exact parameters of the heavy holes were difficult to extract.

After 'activation' annealing of non-implanted samples, the basic set of carriers for all the samples remained the same, yet samples reacted to this annealing differently. For example, in sample *C* we observed substantial increase in the mobility of high-mobility electrons (up to μ_n = 115,000 cm^2 / (V·s), see curve *2* in Fig. 2(b)) and their partial conductivity (σ_n = 70.6 (Ohm·cm)$^{-1}$) with their concentration remaining at the same level (n = 3.8·10^{15} cm^{-3}). This increase in mobility and conductivity can be explained by the partial annealing of structural defects, namely, stacking faults [18]. In samples *A* and *B*, however, activation annealing of non-implanted films reduced both the concentration of high-mobility electrons (approx. twofold) and their mobility (curve *2* in Fig. 1(a)). This suggested that the first, high-temperature, step of the activation annealing of these samples not only produced V_{Hg} in the *n*–type 'base', but also activated some acceptor-like residual defects/dopants, which increased the electrical compensation and lead to the decrease in mobility due to the increase in the number of scattering centers. Parameters of lower-mobility electrons were affected by the 'activation' annealing insignificantly.

After ion implantation, the conductivity in all three samples was determined by three sorts of electrons: those with high mobility (80,000–100,000 cm^2 / (V·s)), mid-mobility (10,000–20,000 cm^2 / (V·s)), and low mobility (3,000–5,000 cm^2 / (V·s)). The total conductivity due to holes was less than 2%, so the parameters of the heavy holes were difficult to extract.

Due to the variations in indium doping level in films *A*, *B* and *C*, we have found the properties of as-implanted samples cut from these films to be different. For example, in film *C* after the implantation the conductivity was dominated by high-mobility electrons (obviously, those belonging to the *n*-type 'base' doped to 5·10^{15} cm^{-3}). The average concentration of these electrons equaled n_{av} = 4.01·10^{15} cm^{-3} with mobility μ_n = 85,700 cm^2 / (V·s). The next contribution to conductivity was that by the low-mobility electrons with μ_{h2} = 3,590 cm^2 / (V·s) and average concentration n_{avh2} = 2.03·10^{16} cm^{-3} and concentration in the implanted layer with the thickness ~400 nm (determined with TEM) ~4.6·10^{17} cm^{-3}. These parameters suggested that both in *n*- and *p*-type implanted HgCdTe the low-mobility electrons originate in Hg_I captured by dislocation loops [9].

In contrast to sample *C*, in as-implanted samples *A* and *B* conductivity was dominated by electrons with low mobility (μ_{h2} = 4540 cm^2 / (V·s) and μ_{h2} = 4,090 cm^2 / (V·s), respectively). For sample *A*, the average concentration of these electrons was n_{avh2} 2.63·10^{16} cm^{-3}; concentration in the 400 nm-thick layer, 4.8·10^{17} cm^{-3}. So, these electrons obviously belonged to the implanted layer. In all three samples, electrons with mid-mobility were also found, but their contribution to conductivity was small.

After activation annealing of the implanted samples we observed significant changes in the assortments of carriers for all the films. First, the peak corresponding to the low-mobility electrons (~3,500–4,500 cm^2 / (V·s), see curves *4* in Fig. 2) disappeared. This was indicative of the annihilation of the defects that had captured Hg_I, and fully agreed with the data on optical reflectance discussed above (see Fig. 1). TEM studies of as-implanted samples *B* and *C* revealed characteristic patterns of defects; this pattern is shown for sample *B* in Fig. 3(a) while for sample *C* it was reported on in Ref. [8]. In particular, in as-implanted film *B* a top thin (45–50 nm) low-defect layer *A* was followed by a ~120 nm-thick layer B_1 containing 'large' extended defects, such as dislocation loops, and a ~110 nm-thick layer B_2 containing 'smaller' extended defects. These layers were followed by a layer P_1 containing quasi-point defects. After the activation annealing the low-defect layer disappeared (see Fig. 3(b)), while the dislocation loops transformed into single dislocations with higher density (an upper layer B'_1 with thickness ~120 nm) and lower density (a lower layer B'_2 with the thickness ~170 nm). It is possible that optical reflectance is not that sensitive to the presence of single dislocations, but the general pattern of the behavior of the large extended defects, dislocation loops, was clear.

The analysis of the behavior of the mid-mobility electrons was more challenging to perform. These electrons showed off both in the as-grown samples (where they could be associated with transitional substrate/film buffer layer [16,17]) and in as-implanted samples, where they could be related to the formation of implantation-induced quasi-point defects, which also capture Hg_I [9]. Straight after the implantation the concentration of these electrons was two times higher than that in the as-grown samples, but the exact contribution of the two sorts of carriers could not be resolved. Still, after the activation annealing of the implanted samples, the concentration of these electrons was reduced and approached that in the as-grown samples, which indicated that the annealing lead to the annihilation of quasi-point implantation-induced

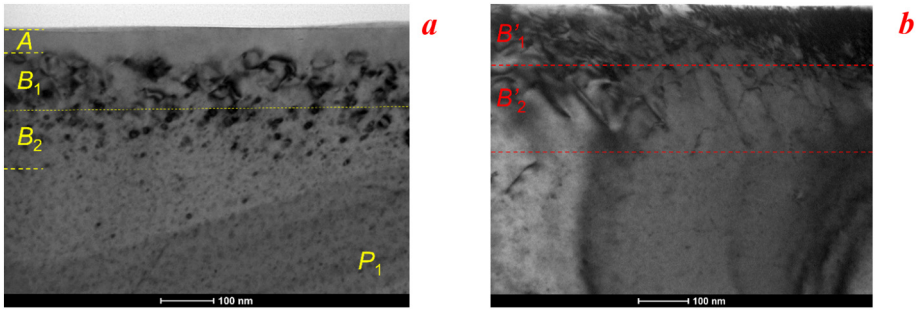

Fig. 3. Bright-field TEM images of the cross-section of sample *B* after ion implantation (*a*) and after post-implantation activation annealing (*b*). Letters *A*, B_1, B_2, P_1, B_1' and B_2' designate layers with defects with various sizes and concentrations.

defects. In Ref. [19], a similar conclusion on the annihilation of these defects as a result of post-implantation activation annealing was made on the basis of the results of the Rutherford backscattering experiments.

Let us now compare the results of activation annealing performed on non-implanted samples and samples after ion implantation. For sample *C*, we have noted some increase in the electron mobility and conductivity in the annealed non-implanted samples, which could be attributed to the annihilation of stacking faults [18]. Annealing of the implanted samples also lead to some increase in mobility (up to μ_n = 97,300 cm^2 / (V·s)) with both the concentration and partial conductivity of these electrons slightly decreasing. Samples *A* and *B* behaved similarly after activation annealing of the as-grown samples, but differently after the annealing of the implanted samples. In sample *A*, electrical parameters of the two annealed (non-implanted and implanted) samples were very similar. In sample *B*, the annealing of the implanted samples lead to the twofold decrease in the concentration of high-mobility electrons accompanied by a significant increase in mobility and partial conductivity as compared to those in the annealed non-implanted sample. This behavior requires additional studies. As to the parameters of the heavy holes in the implanted and annealed samples, the primary MSEs of these samples clearly showed a peak corresponding to heavy holes (see curves *4* in Fig. 2 at mobility values close to zero). The exact degree of the electrical activation of arsenic was a bit challenging to access in all the samples, yet the value of heavy hole concentration of $1.8{\cdot}10^{18}$ cm^{-3} obtained for sample *A* agreed very well with the acceptor concentration determined in the surface layer of this sample with the admittance measurements [20] and with the average concentration of implanted arsenic ions determined with SIMS ($2.7{\cdot}10^{18}$ cm^{-3}). Samples *A* and *B* that were implanted with arsenic and subjected to activation annealing, were additionally subjected to '*p*-type' annealing. It was expected that with the 'base' layer transformed under this annealing from *n*- to *p*-type, the contribution to electrical conductivity of the implanted p^+-type layer would be more substantial. However, the expectations were not met, as after the annealing, both samples became 'typically *p*-type' with the set of carriers basically containing just two types of holes. For sample *A*, concentration, mobility and partial conductivity of the heavy and light holes equaled, respectively, p = $1.92{\cdot}10^{16}$ cm^{-3}, μ_p = 380 cm^2 / (V·s), p_l = $2.8{\cdot}10^{13}$ cm^{-3}, μ_{pl} = 6,440 cm^2 / (V·s). For sample *B*, these parameters equaled, respectively, p = $2.05{\cdot}10^{16}$ cm^{-3}, μ_p = 410 cm^2 / (V·s); p_l = $2.09{\cdot}10^{13}$ cm^{-3}, μ_{pl} = 7,090 cm^2 / (V·s). With the graded-gap surface layer removed with chemical etching, the parameters did not change. Parameters of electrons were difficult to resolve due to their low (~2%) contribution to conductivity.

The data gathered in the course of the studies are summarized in Figure 4 for high-mobility electrons. As can be seen, in sample *C* their concentration (Figure 4(a)) did not vary much from treatment to treatment, yet in samples *A* and *B* it significantly dropped after activation annealing performed on non-implanted samples. As discussed earlier, this could be related to partial electrical compensation of donors by uncontrollable background acceptors that were activated during the annealing. This was confirmed by the substantial drop in the mobility after this treatment (Figure 4(b)). After '*p*-type' annealing, the electron concentration also naturally dropped due to the generation of large number of V_{Hg}, acceptors.

The difference in the behavior of the concentration and mobility in samples *A*, *B* and *C* can obviously be related to different C_{In} values in the initial samples. It is clear that low doping is not preferable, as it does not allow one to fully control the electrical properties of the 'base' of p^+-*n* photodiodes due to the possible effect of residual acceptors. On the other hand, the value of $C_{In} \approx 5{\cdot}10^{15}$ cm^{-3} in sample *C* is close to the point where electron concentration in the *n*-'base' starts affecting the value of dark currents in the photodiode [3,4]. Therefore, moderate indium doping ($(2–3){\cdot}10^{15}$ cm^{-3}) is preferable.

Summarizing, we demonstrated that activation annealing of arsenic-implanted samples did lead to annihilation of extended structural defects (dislocation loops) and electrically active defects associated with the loops. This conclusion was based on the data of both the Hall-effect and optical reflectance studies. The TEM data, however, showed that activation annealing transformed the dislocation loops into single dislocations, which optical reflectance could not detect. It also appeared that activation annealing lead to the annihilation of quasi-point implantation-induced defects. From the point of view of the electrical properties of material, it appeared that activation annealing not only led to the restoration of the properties of *n*-'base', which were affected by generation of V_{Hg} at the high-temperature stage of the annealing, but also could lead to alterations in its electrical properties via activation of background acceptors and modification of the degree of electrical compensation. Finally, though our experiments clearly demonstrated formation, as a result of implantation and annealing, of a *p*-type surface layer, it appeared challenging to fully assess the degree of electrical activation of arsenic in this layer for all the studied samples due to the weak contribution of holes to the conductivity of a p^+-*n* structure with a rather thick *n*-'base'. It seems that this degree can be more easily determined with the admittance studies [20].

4. Conclusion

In conclusion, the results of the Hall-effect studies of modification of HgCdTe surface properties with arsenic ion implantation and thermal annealing showed that the formation of implantation-induced extended defects proceeds similarly in samples with *p*- and *n*-type conductivity of the photodiode 'base'. As a result of activation annealing, a high degree of arsenic activation was achieved as well as complete annihilation of the extended defects (dislocation loops), quasi-point defects, and related radiation donor centers responsible for the appearance of electrons with low and medium mobility was observed. Still, while in some samples activation annealing eventually did not change the electrical properties of the *n*-'base' and kept them very similar to those of the original (as-grown) material, in some cases, the annealing led to the

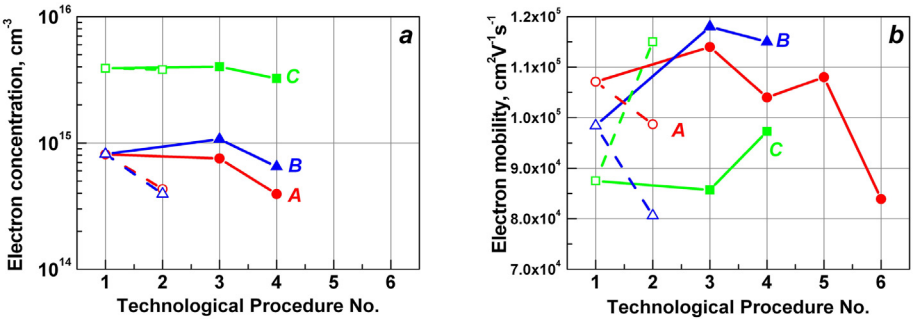

Fig. 4. Concentration (*a*) and mobility (*b*) of the high-mobility electrons in the studied samples: after the growth (*1*); after 'activation' annealing performed on the non-implanted samples (*2*); after ion implantation (*3*); after activation annealing of the implanted sample (*4*); after '*p*-type' annealing of the implanted and activation-annealed sample (*5*), after the removal of the graded-gap surface layer from the annealed sample (*6*).

modification of these properties due to the activation of uncontrolled acceptor defects and changes in the degree of electrical compensation.

CRediT authorship contribution statement

A.G. Korotaev: Conceptualization, Methodology, Writing - review & editing, Validation. **I.I. Izhnin:** Conceptualization, Methodology, Data curation, Writing - review & editing, Validation. **K.D. Mynbaev:** Conceptualization, Methodology, Writing - original draft, Validation. **A.V. Voitsekhovskii:** Conceptualization, Methodology, Writing - original draft, Validation. **S.N. Nesmelov:** Formal analysis, Writing - review & editing, Validation. **S.M. Dzyadukh:** Formal analysis, Writing - review & editing, Validation. **O.I. Fitsych:** Formal analysis, Writing - review & editing, Validation. **V.S. Varavin:** Formal analysis, Writing - review & editing, Validation. **S.A. Dvoretsky:**Conceptualization, Methodology, Writing - original draft. **N.N. Mikhailov:** Conceptualization, Methodology, Writing - original draft. **M.V. Yakushev:** Conceptualization, Methodology, Writing - original draft. **O.Yu. Bonchyk:** Formal analysis, Writing - review & editing, Validation. **H.V. Savytskyy:** Formal analysis, Writing - review & editing, Validation. **Z. Swiatek:** Formal analysis, Writing - review & editing, Validation. **J. Morgiel:** Formal analysis, Writing - review & editing, Validation.

Declaration of competing interest

The authors declare that they have no known competing financial interests or personal relationships that could have appeared to influence the work reported in this paper.

References

[1] W. Lei, J. Antoszewski, L. Faraone, Progress, challenges, and opportunities for HgCdTe infrared materials and detectors, Appl. Phys. Rev. 2 (2015) 041303, , https://doi.org/10.1063/1.4936577.
[2] L.O. Bubulac, D.S. Lo, W.E. Tennant, D.D. Edwall, J.C. Robinson, Boron and indium ion implanted junctions in HgCdTe grown on CdTe and CdTe/Al_2O_3, J. Vac. Sci. Technol. A 4 (1986) 2169, https://doi.org/10.1116/1.574049.
[3] L. Mollard, G. Destefanis, G. Bourgeois, A. Ferron, N. Baier, O. Gravrand, J.P. Barnes, A.M. Papon, F. Milesi, A. Kerlain, L. Rubaldo, Status of *p*-on-*n* arsenic-implanted HgCdTe technologies, J. Electron. Mater. 40 (2011) 1830, https://doi.org/10.1007/s11664-011-1692-z.
[4] L. Mollard, G. Destefanis, N. Baier, J. Rothman, P. Ballet, J.P. Zanatta, M. Tchagaspanian, A.M. Papon, G. Bourgeois, J.P. Barnes, C. Pautet, P. Fougeres, Planar *p*-on-*n* HgCdTe FPAs by arsenic ion implantation, J. Electron. Mater. 38 (2009) 1805, https://doi.org/10.1007/s11664-009-0829-9.
[5] J.H. Park, J. Pepping, A. Mukhortova, S. Ketharanathan, R. Kodama, J. Zhao, D. Hansel, S. Velicu, F. Aqariden, Development of high-performance eSWIR HgCdTe-based focal-plane arrays on silicon substrates, J. Electron. Mater. 45 (2016) 4620, https://doi.org/10.1007/s11664-016-4717-9.
[6] C.Z. Shi, C. Lin, Y.F. Wei, L. Chen, M. Zhu, Barrier layer induced channeling effect of As ion implantation in HgCdTe and its influences on electrical properties of *p*–*n* junctions, Appl. Opt. 55 (2016) D101, https://doi.org/10.1364/AO.55.00D101.
[7] C. Lobre, P.H. Jouneau, L. Mollard, P. Ballet, Characterization of the microstructure of HgCdTe with *p*-type doping, J. Electron. Mater. 43 (2014) 2908, https://doi.org/10.1007/s11664-014-3147-9.
[8] O.Yu. Bonchyk, H.V. Savytskyy, Z. Swiatek, Y. Morgiel, I.I. Izhnin, A.V. Voitsekhovskii, A.G. Korotaev, K.D. Mynbaev, O.I. Fitsych, V.S. Varavin, S.A. Dvoretsky, D.V. Marin, M.V. Yakushev, Nano-size defects in arsenic-implanted HgCdTe films: a HRTEM study, Appl. Nanosci. 9 (2019) 725, https://doi.org/10.1007/s13204-018-0679-y.
[9] I.I. Izhnin, K.D. Mynbaev, A.V. Voitsekhovsky, A.G. Korotaev, I.I. Syvorotka, O.I. Fitsych, V.S. Varavin, S.A. Dvoretsky, N.N. Mikhailov, V.G. Remesnik, M.V. Yakushev, Z. Swiatek, J. Morgiel, O.Yu. Bonchyk, H.V. Savytskyy, Arsenic-ion implantation-induced defects in HgCdTe films studied with hall-effect measurements and mobility spectrum analysis, Infr. Phys. Technol. 98 (2019) 230, https://doi.org/10.1016/j.infrared.2019.03.019.
[10] I.I. Izhnin, I.I. Syvorotka, O.I. Fitsych, V.S. Varavin, S.A. Dvoretsky, D.V. Marin, N.N. Mikhailov, V.G. Remesnik, M.V. Yakushev, K.D. Mynbaev, A.V. Voitsekhovsky, A.G. Korotaev, Electrical profiling of arsenic-implanted HgCdTe films performed with discrete mobility spectrum analysis, Semicond. Sci. Technol. 34 (2019) 035009, , https://doi.org/10.1088/1361-6641/aafc6a.
[11] M.V. Yakushev, D.V. Brunev, V.S. Varavin, V.V. Vasilyev, S.A. Dvoretskii, I.V. Marchishin, A.V. Predein, I.V. Sabinina, Yu.G. Sidorov, A.V. Sorochkin, HgCdTe heterostructures on Si(310) substrates for MWIR infrared photodetectors, Semiconductors 45 (2011) 385–391, https://doi.org/10.1134/S1063782611030250.
[12] P.A. Bakhtin, S.A. Dvoretskii, V.S. Varavin, A.P. Korobkin, N.N. Mikhailov, I.V. Sabinina, Yu.G. Sidorov, Effect of low-temperature annealing on electrical properties of *n*-HgCdTe, Semiconductors 38 (2004) 1172, https://doi.org/10.1134/1.1808823.
[13] H. Arwin, D.E. Aspnes, Nondestructive analysis of $Hg_{1-x}Cd_xTe$ (x = 0.00, 0.20, 0.29, and 1.00) by spectroscopic ellipsometry. II. Substrate, oxide and interface properties, J. Vac. Sci. Technol. A 2 (1984) 1316, https://doi.org/10.1116/1.572401.
[14] P. Koppel, Visible and ultraviolet reflectivity of $Hg_{1-x}Cd_xTe$, J. Appl. Phys. 57 (1985) 1705, https://doi.org/10.1063/1.334441.
[15] S.A. Dvoretsky, N.N. Mikhailov, V.G. Remesnik, N.Kh. Talipov, Using reflection spectroscopy for assessing structural perfection of CdTe/GaAs films and $Cd_xHg_{1-x}Te$ crystals, Avtometriya 5 (1998) 73–77 (Russian).
[16] V.S. Varavin, A.F. Kravchenko, Yu.G. Sidorov, A study of galvanomagnetic phenomena in MBE-grown *n*-$Cd_xHg_{1-x}Te$ films, Semiconductors 35 (2001) 992, https://doi.org/10.1134/1.1403562.
[17] V.V. Bogoboyashchyy, S.A. Dvoretsky, I.I. Izhnin, N.N. Mikhailov, Yu.G. Sidorov, F.F. Sizov, V.S. Varavin, V.A. Yudenkov, Properties of MBE $Cd_xHg_{1-x}Te$/GaAs structures modified by ion-beam milling, Phys. Status Solidi C 1 (2004) 355 https://doi.org/10.1002/pssc.200303947.
[18] I.I. Izhnin, A.I. Izhnin, H.V. Savytskyy, M.M. Vakiv, Y.M. Stakhira, O.I. Fitsych, M.V. Yakushev, A.V. Sorochkin, I.V. Sabinina, S.A. Dvoretsky, Yu.G. Sidorov, V.S. Varavin, M. Pociask-Bialy, K.D. Mynbaev, Defect structure of HgCdTe films grown by molecular beam epitaxy on Si substrates, Semicond. Sci. Technol. 27 (2012) 035001, , https://doi.org/10.1088/0268-1242/27/3/035001.
[19] C. Lobre, D. Jalabert, I. Vickridge, E. Briand, D. Benzeggouta, L. Mollard, P.H. Jouneau, P. Ballet, Quantitative damage depth profiles in arsenic implanted HgCdTe, Nucl. Instrum. Meth. B. 313 (2013) 76, https://doi.org/10.1016/j.nimb.2013.07.019.
[20] A.G. Korotaev, A.V. Voitsekhovskii, I.I. Izhnin, K.D. Mynbaev, S.N. Nesmelov, S.M. Dzyadukh, V.S. Varavin, S.A. Dvoretsky, N.N. Mikhailov, M.V. Yakushev, G.Yu. Sidorov, Admittance studies of modification of HgCdTe surface properties with ion implantation and thermal annealing. 21st International Conference on Surface Modification of Materials by Ion Beams. August 25–30, 2019, Tomsk Russia. Abstract Book. Mozart, Tomsk, Russia. P. 147.